Penerbit Akademia Baru

Journal of Advanced Research in Fluid Mechanics and Thermal Sciences

Journal homepage: www.akademiabaru.com/arfmts.html
ISSN: 2289-7879

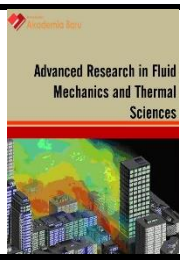

Statistical Description of The Turbulent Round Jet Developing Region Along Its Centerline

Open Access

Mohd Rusdy Yaacob[1,2,*], Preben Buchhave[3], Clara Marika Velte[4]

[1] Faculty of Electrical Engineering, Universiti Teknikal Malaysia Melaka, Hang Tuah Jaya, 76100 Durian Tunggal, Melaka, Malaysia
[2] Center for Advanced Research on Energy (CARe), Universiti Teknikal Malaysia Melaka, Hang Tuah Jaya, 76100 Durian Tunggal, Melaka, Malaysia
[3] Intarsia Optics, Sønderskovvej 3, 3460 Birkerød, Denmark
[4] Department of Mechanical Engineering, Technical University of Denmark, 2800 Kgs. Lyngby, Denmark

ARTICLE INFO

Article history:
Received 1 August 2019
Received in revised form 11 November 2019
Accepted 19 November 2019
Available online 31 December 2019

ABSTRACT

Due to the technical measurement difficulties, analysis on the developing region of a turbulent round jet has been omitted despite its vast significance in explaining the establishment of the fully developed counterpart. With a self-developed novel and sophisticated laser Doppler system that can accurately measure high turbulence intensity flow with high spatial resolution and dynamics range, a turbulent round jet is mapped in terms of statistical moments along the centerline throughout and beyond the developing region. About 25-30 jet exit diameters downstream, turbulence begins to approach the fully developed state where the mean velocity and variance develop in parallel in a seeming equilibrium. Turbulence intensity is consequently observed to initially increase before levelling out when approaching the fully developed state. The downstream development of the measured spatial energy spectra and second-order structure functions further support these observations in that they begin to develop the Kolmogorov characteristic -5/3 and 2/3 slopes in the inertial subrange within the downstream distance of 25-30 jet exit diameters. The dissipation can be to a reasonable approximation extracted from the third-order structure functions from about 20 jet exit diameters and further downstream. The results should be useful for development of analytic and numerical turbulence models.

Keywords:
Turbulent round jet; Centerline measurements; Laser Doppler anemometer; turbulence modelling

1. Introduction

The axisymmetric turbulent round jet is a classical turbulent flow that exhibits a wide range of dynamical variations [1]. While the fully developed jet has been extensively studied in the past [2–8], the developing region has often been omitted from the analysis since the transitional development and high intensity and shear in this region present additional measurement technical difficulties and since equilibrium and similarity in a general sense (defined as similar development of the first and second-order statistics) have been assumed not to be valid. At the same time, a deeper

* *Corresponding author.*
E-mail address: rusdy@utem.edu.my (Mohd Rusdy Yaacob)

understanding of the developing region is vital for understanding how the state in the fully developed region is reached (e.g., if there exists a dependency upon initial conditions)[9–11] and, not least, how to accurately model it in computer simulations. Of particular interest is testing the (range of) validity of the Kolmogorov hypotheses within this region and providing data for validation of analytical and computational models.

In terms of accuracy of measurements, the centerline region is considered less challenging compared to the shear region, where the velocity fluctuations and turbulence intensity are much larger [12,13]. However, measurements along the jet centerline can be of significant interest in mapping the energy cascade in the centerline region. In general, a mapping of the static and dynamic statistics of the velocity field in the developing jet region using high accuracy measurements can be of significant interest in synthesizing analytical and numerical models for developing flows. It is therefore of interest to perform these centerline measurements in the developing jet region using a novel and sophisticated laser Doppler anemometry system [14], which has been proven to function robustly even in the more difficult high shear and intensity regions of the jet [15,16].

Herein, we present laser Doppler anemometry measurements of the cascade development along the jet centerline, including the static moments, spatial kinetic energy spectra as well as spatial second- and third-order structure functions. From the latter, the dissipation time and length scales have been extracted along the lines of Kolmogorov [1720] as a function of downstream distance, where applicable. The corresponding temporal/spatial Kolmogorov and integral scales obtained from the measurements are also presented.

2. Instrumentation and Measurements

2.1 Traversable Turbulent Round Jet

The design and interior of the jet generator box, which was fabricated in the DTU workshop, replicates the one used by [12,21]. Inside the box, baffles with foam coating have been inserted to even out large disturbances, followed by screens to remove remaining fluctuations in the stream. The nozzles following consist firstly of a trumpet nozzle (Figure 1(a)), which is tooled to transition to a pipe connecting it to an outer nozzle (Figure 1(b)). The outer nozzle has an inner diameter of 32 mm, an exit diameter, D=10 mm and a fifth-order polynomial contraction that allows a uniform flow [22] resulting in a well-approximated top-hat velocity profile [23].

The jet generator box is mounted on two linear traversing units (stacked to each other) for maneuvering the measurement volume to the desired measurements points throughout the ensuing jet in the streamwise and transverse directions. Each unit is equipped with limit switches and a stepper motor from ISEL Automation. An iMC-S8 stepper motor controller is permanently connected to a computer to drive the motors in micro stepping mode. A *RemoteWIN* software is installed in the computer to operate the traversing units in a semi-auto mode. In order to match the distance traversed on the hardware and the software parts, the number of steps per revolution and spindle elevation needs to be set according to the datasheets.

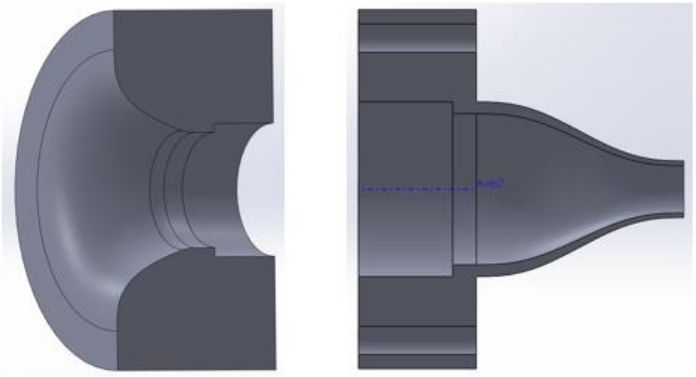

(a) (b)

Fig. 1. (a) Trumpet nozzle (b) Outer nozzle with fifth-order polynomial contraction. The two nozzles are connected by a geometrically smoothly transitioning pipe that penetrates the jet generator box wall

2.2 Laser Doppler System

Laser Doppler anemometry (LDA) is a non-intrusive method for measuring the velocity of a flow. By seeding the working fluid with seeding particles with an optimal size in terms of faithfulness in tracing the flow and light scattering properties [24], the velocity of each particle can be acquired and assumed to represent the flow velocity to an acceptable approximation [252]. The measuring volume is created when a coherent laser beam is split into two and focused into a common point using a converging lens (see Figure 2**Error! Reference source not found.**). Where they intersect, a fringe pattern is formed from the two coherent beams and the Doppler frequency of the seeding particles can be measured [27–29]. Before the beams intersect, each beam passes through a Bragg cell with an effective frequency shift difference between the beams, f_s=3 MHz to resolve any negative component of the velocity in the measured flow [30,31]. After compensating for the differential frequency shift, the velocity can be calculated by

$$u = \frac{\lambda f_D}{2sin\left(\theta/_2\right)} = f_D d_f \tag{1}$$

where λ is the wavelength of the laser (532 nm), ϑ is the beam angle and f_D is the Doppler frequency of the moving particle. d_f is the fringe spacing in the measuring volume.

$$d_f = \frac{\lambda}{2\sin(\theta/_2)} \tag{2}$$

In order to obtain a sufficiently high spatial resolution to convincingly resolve the Kolmogorov length scale throughout the measurement domain, a converging lens with a focal length of 200 mm was used. This resulted in a measuring volume of the order of 90 μm and a sufficiently dense fringe spacing that produced good quality bursts for Doppler frequency detection compared to the seeding particle size. Based on this measuring volume, the smallest resolvable length scale can therefore be computed. From

$$k\eta_{Kol} = \frac{2\pi}{\lambda}\eta_{Kol} = 1 \tag{3}$$

at which the dissipation is approximately 99% resolved, the smallest resolvable Kolmogorov length scale using our instrument can be calculated by

$$\eta'_{Kol} = \frac{\lambda}{2}\frac{1}{\pi} \quad (4)$$

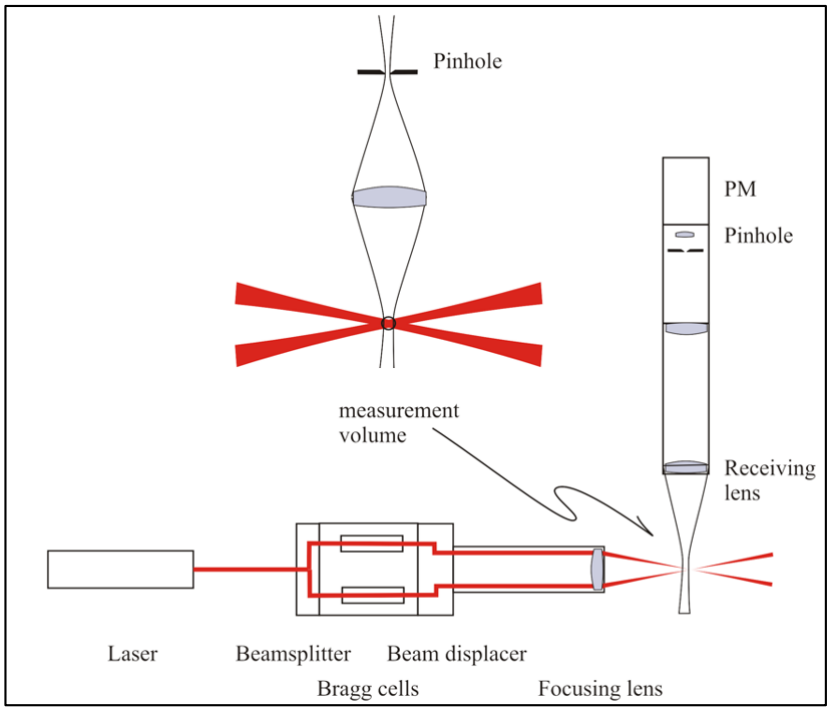

Fig. 2. Schematic drawing (side view) of the LDA setup

Since the laser Doppler anemometer is operating in burst-mode, the processor cannot process more than one seeding particle in the measuring volume at a time, since this would result in overlapping bursts with in general different phases and faulty residence times. A smaller measuring volume thus enables a higher spatial seeding density, since for a smaller volume the probability of having more than one particle in the measuring volume is lowered. This consequently enables a higher spatial seeding density (thereby a higher data rate), and thus a wider spectral turbulent kinetic energy content with a higher signal-to-noise ratio [32].

For the same purpose, the photodetector is mounted at a 45° forward scattering angle (see Figure 3) from the transmitting optics axis to allow an optimum between sufficient amount of light scattered by each particle and an effective reduction of the detected region of the measuring volume [33]. Thereby, the effective (detectable) measuring volume is reduced from an ellipsoid to a nearly spherical shape. This configuration has led us to attach both traversing units to the jet box instead of traversing the optical head, which sensitivity to misalignment may otherwise cause erroneous or complete dropout of measurements as observed by the photodetector.

To obtain quality measurements, it is thus vital that the transmitting and receiving optics of the laser Doppler anemometer is carefully aligned. The optics inside the transmitting optics must be tilted accordingly in a way that the two beams perfectly overlap at the desired focal point. Furthermore, the photodetector needs to be carefully aligned with respect to the MV until a high-quality burst is observed. This is in practice best achieved by observing the voltage signal from the photomultiplier (detector) live on an oscilloscope. The LDA optics and processing are described in great detail in [14,16,34].

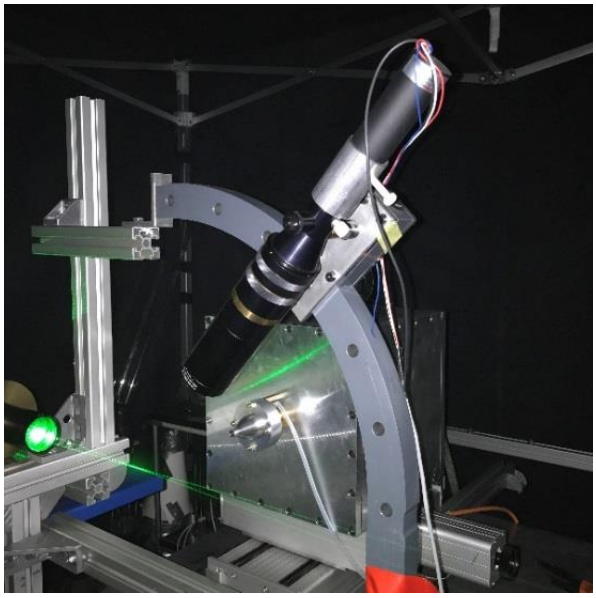

Fig. 3. LDA system in a large tent (3 x 5.8 x 3.1 m^3)

3. Computation of Turbulence Statistics

Upon data processing, the software outputs the value of the residence (transit) time, arrival time and instantaneous streamwise velocity of each detected burst. The mean streamwise velocity, $\bar{u}_i$ and the velocity variance, $\overline{u_i^2}$ at each measurement point are determined based on residence time-weighting [12,35–37].

$$\bar{u} = \frac{\sum_{n=0}^{N-1} u_i(t_n)\Delta t_n}{\sum_{n=0}^{N-1} \Delta t_n} \tag{5}$$

$$\overline{u^2} = \frac{\sum_{n=0}^{N-1} [u_i(t_n) - \bar{u}_i]^2 \Delta t_n}{\sum_{n=0}^{N-1} \Delta t_n} \tag{6}$$

where Δt_n is the residence time for the n^{th} realization. It has been shown from first principles to produce non-biased statistics of the LDA burst signal and experimental validation supports the theoretical deductions [12,15].

The time records acquired from the measurements are mapped to spatial records based on the convection record principle in order to devotedly represent the energy content of the spatial structures [15].

$$s(t) = \int_0^t |\bar{u}(x_0, t')| dt' \tag{7}$$

where s is the scalar length of accumulated convection elements for fluid passing through the measuring volume, x_0 is the location of the fixed measuring volume and $\bar{u}$ is the instantaneous velocity vector at a time, t'. This method provides an exact mapping of what Taylor's hypothesis only approximates, where the instantaneous velocity magnitude is used instead of the averaged streamwise velocity component. One can consequently measure kinetic energy spectra in the wave number (spatial) domain that display the true distribution of spatial scales instead of the one displayed in the frequency (temporal) domain. The latter is unreliable towards the unsteady convection of the large scales [38], among other factors.

The spatial kinetic energy spectra are computed by

$$S_i(k) = \frac{1}{L}\hat{u}_i(k)\hat{u}_i(k)^* \tag{8}$$

where $\hat{u}_k(k)$ is the Fourier transform of $u_i(s)$ and *L* is the length of the spatial record. Note that also the Fourier transform must be computed using residence time weighting for laser Doppler measurements [12,35–37]. The spatial second-order and third-order structure functions are also computed based on the (residence time averaged) convection record, which are expressed respectively by

$$S_2(\ell_s) = \langle(\bar{u}(s+\ell_s) - \bar{u}(s))^2\rangle \tag{9}$$

$$S_3(\ell_s) = \langle(\bar{u}(s+\ell_s) - \bar{u}(s))^3\rangle \tag{10}$$

where ℓ_s is the spatial separation along the *s*-record and the < >-brackets denote ensemble averaging.

In his seminal papers, Kolmogorov assumed local (i.e. small and intermediate scale) homogeneity and isotropy as well as equilibrium and universality [17–20]. These assumptions make the structure function equation reduce into the famous 2/3 and 4/5 laws for the second- and third-order, respectively [39]. The latter is only valid for local homogeneity, isotropy and equilibrium, which supports discarding the measurement points for *x/D*<20 in the following (Results and Discussions) section to meet the last of those conditions. The 4/5 law proposes that the third-order structure functions of velocity increments scale linearly with separation distance ℓ_s [40] as given by

$$S_3(\ell_s) = -\frac{4}{5}\mathcal{E}\ell_s \tag{11}$$

where ε is the mean energy dissipation rate per unit mass and ℓ_s in this case, is also the abscissa on the third-order structure function plot in the following section. As a consequence, if the theory and associated assumptions are valid, the dissipation should be attainable directly from the third-order structure function.

The Kolmogorov time, τ_{Kol} and length scales, η_{Kol} are computed directly from the classic definitions:

$$\tau_{Kol} = \left(\frac{\nu}{\varepsilon}\right)^{1/2} \tag{12}$$

$$\eta_{Kol} = \left(\frac{\nu^3}{\varepsilon}\right)^{1/4} \tag{13}$$

where ε is the mean energy dissipation rate per unit mass and *v* is kinematic viscosity of the air.

The integral time scale, T_u is computed from the integral under the covariance function

$$T_u = \int_0^\infty \frac{\overline{u(t)u(t+\tau)}}{\overline{u^2}} d\tau \tag{14}$$

By using Taylor's hypothesis, the spatial counterpart, L_u is estimated by multiplying T_u with the local mean velocity. This hypothesis is assumed to be valid since measurements were performed along the jet centreline, where turbulence intensities are relatively low [41].

4. Results and Discussions

The downstream profiles along the centerline ($10 \leq x/D \leq 37$) of the local mean streamwise velocity and the velocity variance are presented in Figure 4. In general, the velocity decays downstream, as expected [42], where a faster decay occurs in the intermediate field (developing region) compared to the fully developed region, as also being observed in [23,43]. The velocity variance has a similar close to inversely proportional development with downstream distance.

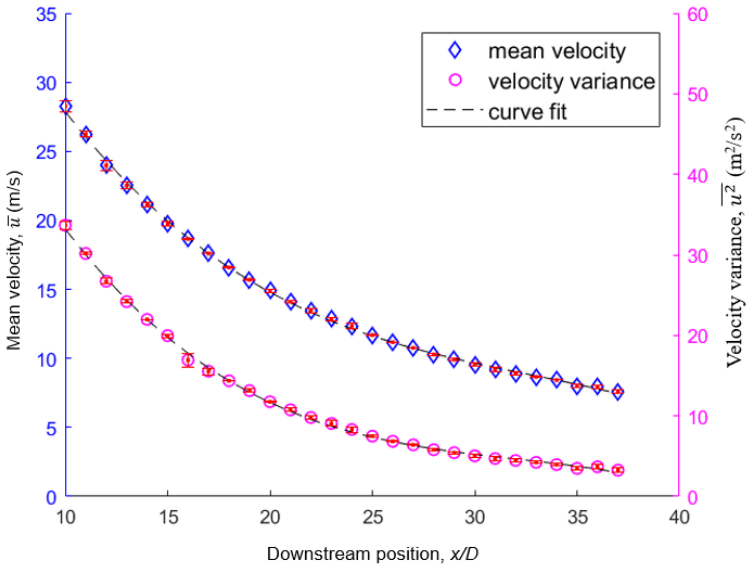

Fig. 4. The downstream profiles (with error bars) of local mean streamwise velocity and streamwise velocity variance with corresponding third-order polynomial curve fits. Coefficient values for the profiles

To simplify the comparison, the normalized inverse of the local mean streamwise velocity and the velocity variance within the range of $10 \leq x/D \leq 37$ are shown in Figure 5. It is immediately observed, that the inverse mean velocity displays a close to linear behavior even in the developing region $10 \leq x/D \leq 30$, whereas the velocity variance clearly is not fully developed until approximately 24 jet exit diameters downstream of the jet exit. Linear curve fits are displayed within the ranges that crudely represent the linear self-preserving regions, e.g., $x/D \geq 20$ and $x/D \geq 24$ for the mean velocity and variance, respectively. The profile demonstrates proportionality between the scaled inverse centerline mean velocity and x/D as suggested by [42] in describing the far field evolution in the jet.

From the linear fit of the inverse mean velocity, the virtual origin is determined to x_0=2.3D and the decay constant to B_u=6.6, based on the calculation at x/D=30. These results are compared to the ones obtained in the previous studies of turbulent round jets of different Reynold numbers, downstream range and using different measurement techniques (see Table 1). Slight deviations compared to our results are most likely due to the different nozzle geometries (and other initial conditions variations) and the different measurement techniques used. The Reynolds number is known not to affect the spreading rate or the decay constant of turbulent round jets [44]. It is particularly interesting to note, that the inverse variance seems to originate from a different point (x/D=15.6) than the inverse average centerline velocity. The normalized inverse of the RMS velocity is also plotted, which linear self-preserving region is similar to that of the local mean streamwise velocity, i.e., $x/D \geq 20$ (see Figure 6). In this case, the origin of the inverse RMS velocity is found to be approximately at x/D=1.27.

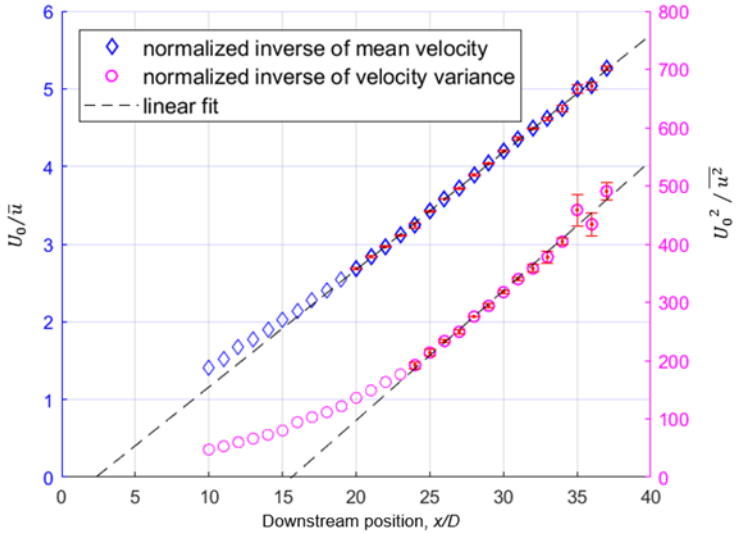

Fig. 5. The normalized inverse of the local mean streamwise velocity and velocity variance, with linear fits and corresponding error bars, covering the points within the estimated linear regions. U_0 is the jet exit velocity ≈ 40 m/s. The linear fit line is extrapolated until it intercepts the x-axis

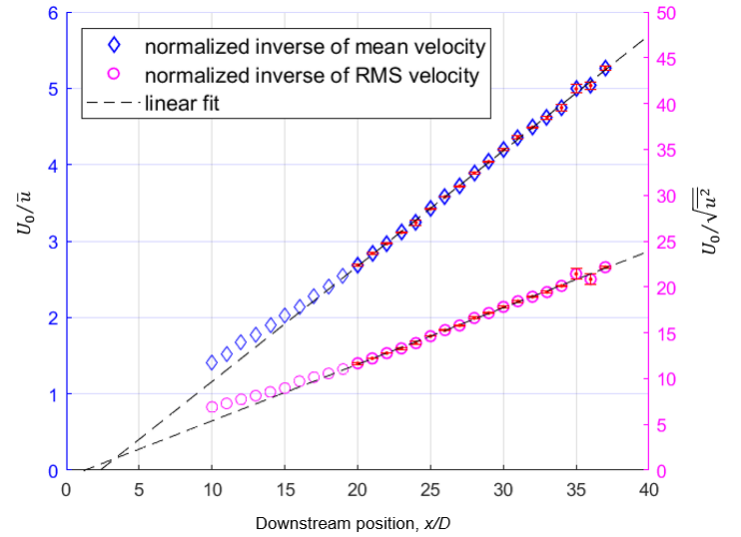

Fig. 6. The normalized inverse of the local mean streamwise velocity and velocity variance, with linear fits and corresponding error bars, covering the points within the estimated linear regions. U_0 is the jet exit velocity ≈ 40 m/s. The linear fit line is extrapolated until it intercepts the x-axis

The streamwise turbulence intensity profile along the centerline is plotted in Figure 7, in terms of the ratio between the velocity fluctuations, u' and the mean velocity. The turbulence intensity builds up in the intermediate field (developing region) due to an increasingly higher influence of the large scale Kelvin-Helmholtz instability development in the shear layer [23,43]. The turbulence intensity increases gradually and asymptotes to a nominal value of around 0.23 in the fully developed region, similarly to [5]. This behavior and the asymptotic value are also found to be in close agreement with most of the previous findings accumulated by [45]. Based on the known similarity

scalings for the fully developed turbulent round jet [46], this asymptotic behavior is assumed to be well sustained farther downstream [47].

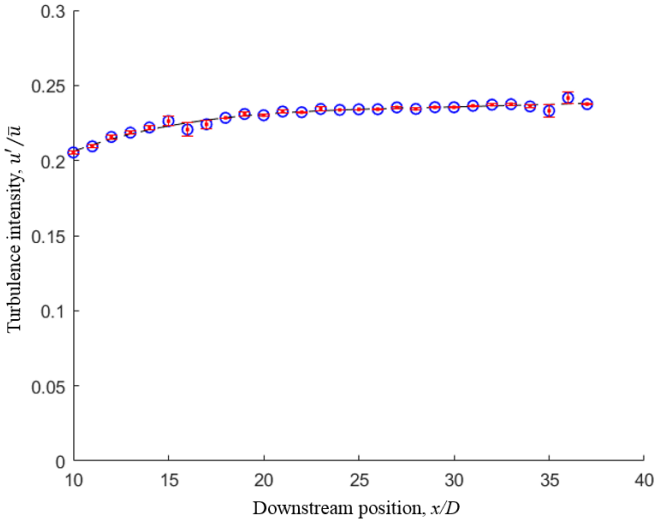

Fig. 7. The downstream development of the streamwise turbulence intensity, $u'/\overline{u}$,

Table 1
The values of Reynolds number and velocity

Authors	*Re*	x_0/D	B_u	*x/D*	Technique
Present study	25000	2.3	6.6	20-37	LDA
[2]	16000	-	6.6	17-27	PIV
[48]	24000	2.5	6.7	15-80	Hot-wire
[5]	100000	4	5.8	15-100	LDA
[49]	20000	3.1	5.9	30-105	PIV
[6]	11000	-	6.06	30-160	Hot-wire

Figure 8 presents the downstream development of the spatial kinetic energy spectra along the jet centerline. Each spectrum is deliberately normalized in the low wave number asymptote to visualize a clearer comparison in term of its shape and slope with respect to the Kolmogorov's -5/3 law. As expected, a wider (assumed existent) inertial subrange is observed in the fully developed region [50]. There is a rapid development from a significant steep deviation in the developing region (intermediate field) to a remarkable resemblance to the -5/3 slope across a wider range in the fully developed counterpart [51]. This observation has also been previously accumulated by [14–16, 52,53] that indicates the possibility of local equilibrium of the small scales in the inertial subrange, at least in this averaged representation, which has been implicitly assumed by Kolmogorov in the fully developed region [50]. Again, one can observe that the spectra have already developed a significant -5/3 range in the assumed inertial subrange at *x/D*≈25-30.

The spatial second-order structure functions based on the convection record method are shown in Figure 9. With downstream position, the width of the variations in the small scales grows, corresponding to the development in the spectra in Figure 8. This clearly demonstrates the downstream development of the turbulence scales. The large scales contain the highest energy in each curve and grow gradually downstream, as denoted by the arrow in the figure. As expected from Kolmogorov's 2/3 law [39] and what has also been obtained by [54], [55], a greater tendency for the curves to follow the 2/3 slope is observed in the fully developed region, compared to those measured

in the developing region where a smaller slope is observed. This indicates that, in the developing region, the cascade process is yet to produce the large velocity increments [16].

According to the Kolmogorov theory, as described above, the dissipation should be directly obtainable from the third-order structure function assuming local homogeneity, isotropy and equilibrium. Although these assumptions are known not to be fulfilled in the jet, and in particular not in the developing region [5], we nevertheless apply the theory herein and compare with other obtained dissipation estimates. The downstream profile of the mean energy dissipation rate per unit mass as obtained from the third order structure functions, ε_{45} is plotted in Figure 10. Measurements upstream of x/D<20 are discarded due to the strong deviations from the underlying assumptions in that region. The individual value of ε_{45} is obtained by best-fitting a 4/5 slope with the corresponding third-order structure function at the small separations, as demonstrated by Eq. (11) and illustrated in Figure 11, specifically at x/D=28 as an example.

In general, ε_{45} decreases downstream with a higher decay rate at the beginning of the fully developed region. This has been compared to the dissipation measured in (Hussein, Capp and George 1994), which present measurement of the dissipation based on the assumption of local axisymmetry of the small scale turbulence (which has been empirically shown to be the best representation in the round turbulent jet). From Figure 21 of the manuscript written in [5], the dissipation along the centerline in the fully developed jet can be empirically scaled as $2\ \varepsilon_{axis}\ (x - x_0) / \overline{u}^3 \approx 0.7$ and has been overlaid in Figure 10 for comparison. Since this estimate is only assumed to be valid in the fully developed jet region, the plot only includes the measurements for x/D≥20. Though there is significant deviation between the two curves in the crudely assumed fully developed region, the two curves have similar trends and seem to converge further downstream in the thoroughly explored fully developed region.

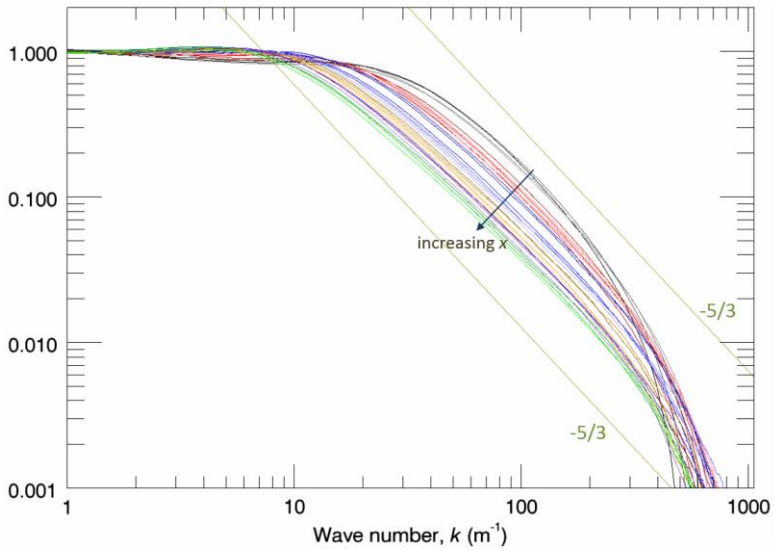

Fig. 8. Downstream development of spatial turbulent kinetic energy (convection record) spectra along the jet centerline. From heavy to light black: x/D=10, 11, 12, 13. From heavy to light red: x/D =14, 15, 16, 17, 18, 19. From heavy to light blue: x/D =20, 21, 22, 23, 24, 25. From heavy to light brown: x/D =26, 27, 28, 29, 30. From heavy to light purple: x/D =31, 32, 33, 34. From heavy to light green: x/D =35, 36, 37. Each spectrum is normalized in the low wave number asymptote to better compare their shapes and slopes with respect to Kolmogorov's -5/3 law

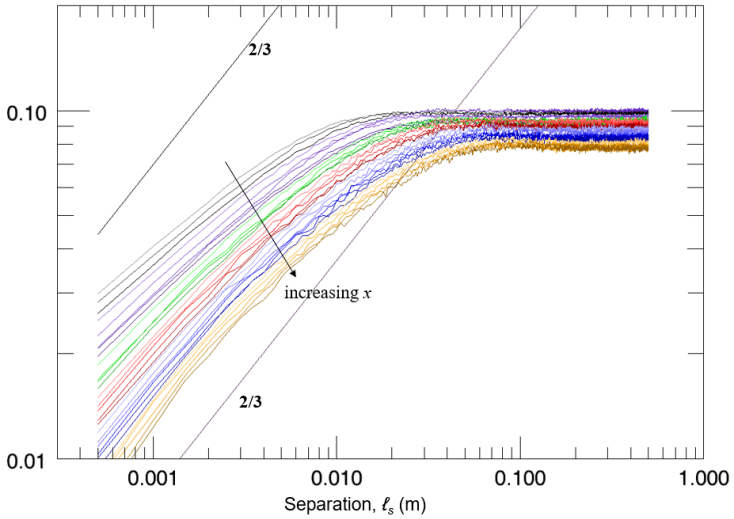

Fig. 9. Spatial second-order structure functions for different downstream positions. From heavy to light brown: x/D=37, 36, 35, 34, 33. From heavy to light blue: x/D=32, 31, 30, 29, 28, 27. From heavy to light red: x/D=26, 25, 24, 23, 22. From heavy to light green: x/D=21, 20, 19, 18. From heavy to light purple: x/D=17, 16, 15, 14, 13. From heavy to light black: x/D=12, 11, 10. Each curve is shifted vertically for a clear comparison of the scales development

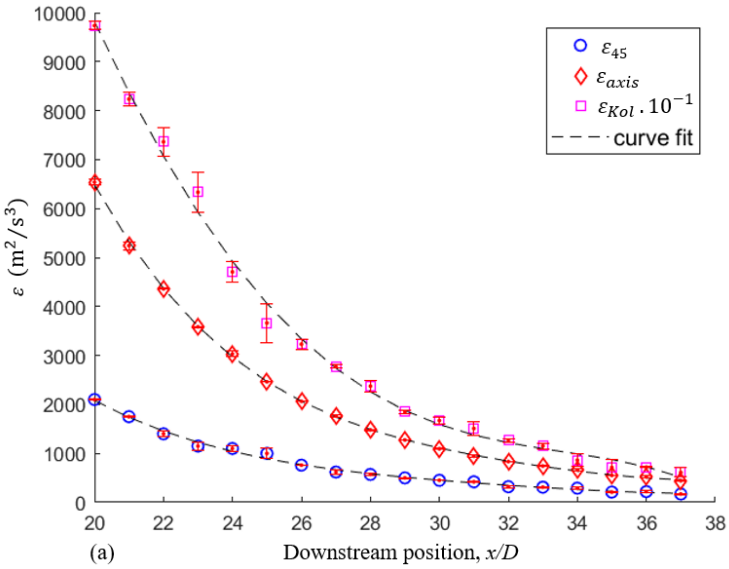

Fig. 10. Downstream evolution of the mean energy dissipation rate per unit mass, ε, with corresponding fourth-order polynomial curve fits. Note that ε_{Kol} is multiplied by 1/10 to compare for any similar trend

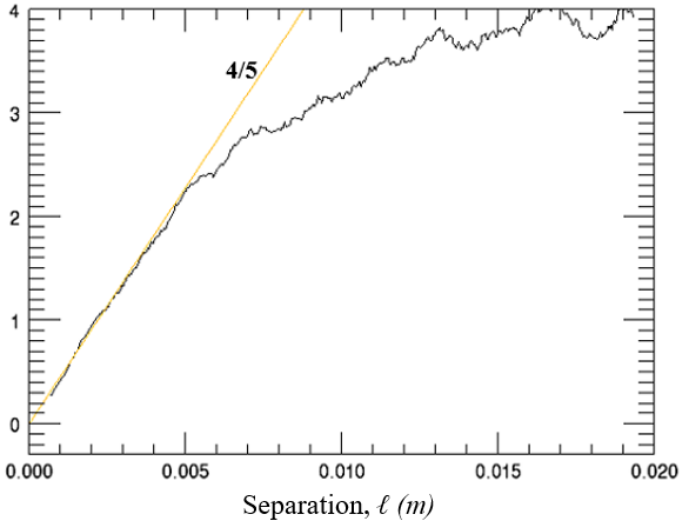

Fig. 11. Spatial third-order structure function at *x/D*=28 (centerline)

The values of dissipation, ε_{45} extracted from the third-order structure function are first used to compute the Kolmogorov scales (both temporal and spatial) as shown in Figure 12. The scales are growing downstream almost linearly, as expected from its inverse proportionality with the dissipation based on Eq. (12) and (13). Similar behavior has also been presented in [56]. The smallest resolvable length scale is also computed based Eq. (4) to be around $\lambda/2 \cdot 1/\pi$ = 28.6 µm. This value is represented by a horizontal *blue* line in Figure 12, which is always way below the linear curve of the Kolmogorov length scales in the measured region. It shows that, with the current spatial resolution of our measurement setup, we should be able to resolve the Kolmogorov scale throughout our measured domain.

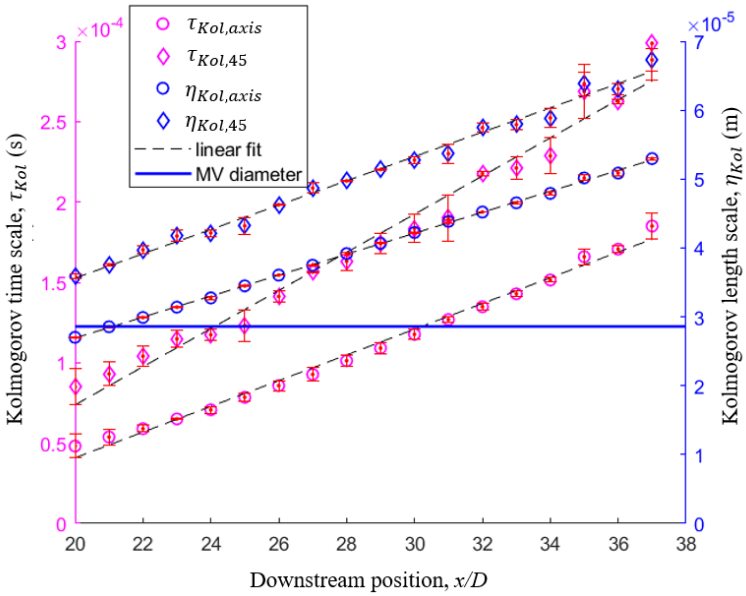

Fig. 12. Downstream evolution of the Kolmogorov time and length scale, with corresponding linear fit. The blue horizontal line represents the smallest resolvable scale of our instrument, i.e., 14.3 µm, which is always below the linear curve of the Kolmogorov length scales

An attempt to estimate the corresponding value of the Taylor microscales has also been done based on its given definition [57]

$$\lambda_L = \sqrt{\frac{\overline{u^2}}{\overline{\left(\frac{du}{dt}\right)^2}}} \tag{15}$$

However, this definition is only clear for a fully turbulent flow that leads to an ambiguity for computations in the intermittent flow. This limitation demands us more time to investigate on any other possible solutions rather than computing the Taylor scale directly from its definition. Another issue with the high frequency domination in the high frequency region also needs to be seriously taken into account since these high frequencies may contaminate the computation of the Taylor scales. Nevertheless, in general, the spatial scales are expected to grow and slow down downstream as what we can observe from the downstream profiles of the Kolmogorov and integral scales in as Figure 12 and Figure 13, respectively.

From the values of the integral length scale, L_u obtained, the Kolmogorov dissipation estimate, ε_{Kol} is also computed by $\overline{u^3}/L_u$, which values have been overlaid together with ε_{45} and ε_{axis} in Figure 10. Though there is significant deviation between the three curves in the crudely assumed fully developed region ($x/D \geq 20$), each curve exhibits similar trends in both scales and seem to converge further downstream in the well-known fully developed region. Similar plots are also constructed in logarithmic scale as in Figure 14. In this case, each dissipation estimate exhibits a linear trend downstream with different decay rates denoted by the exponent of x/D. It is also remarkable that the dissipation from the 4/5 law, $\varepsilon_{45,}$ (which assumptions are not fulfilled) does not agree with the dissipation estimate epsilon, ε_{Kol}, which are both central results from the same Kolmogorov theory. If the theory was correct, the assumptions should be valid AND the two dissipation estimates should give (at least approximately) the same values.

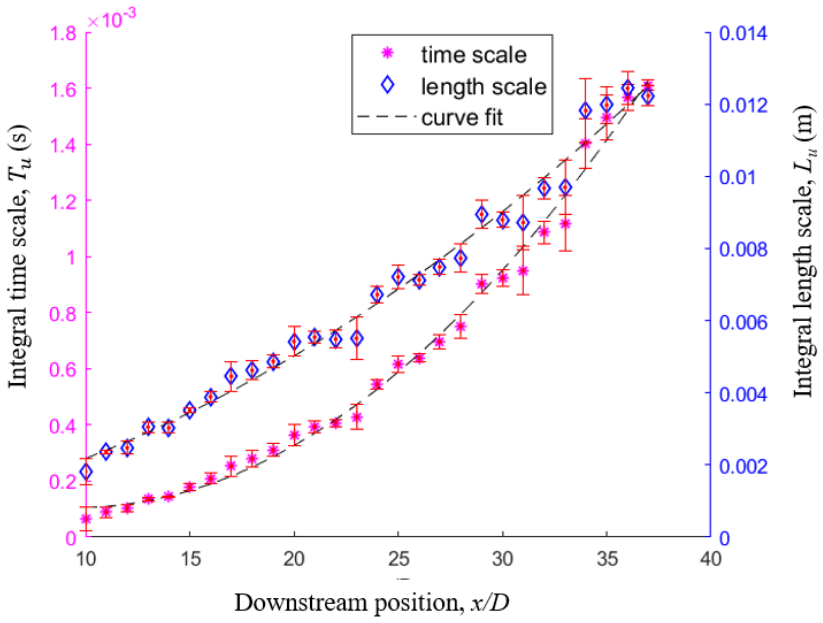

Fig. 13. Downstream evolution of the integral time and length scale, with corresponding second-order polynomial fit

The most credible estimate would be the axisymmetric one, ε_{axis}, since it has been empirically established in [5,58]. The values of this estimate are therefore used to recalculate the Kolmogorov length scales, $\eta_{Kol,axis}$ and time scales, $\tau_{Kol,axis}$ that have been overlaid in Figure 12. In this case, the values of $\eta_{Kol,axis}$ measured are still beyond and equal to the smallest resolvable length scale (horizontal *blue* line) except for the only one at x/D=20, which value is just very slightly smaller. This exception however can still be acceptable considering that the values of the MV and $\eta_{Kol,axis}$ are determined only based on estimations.

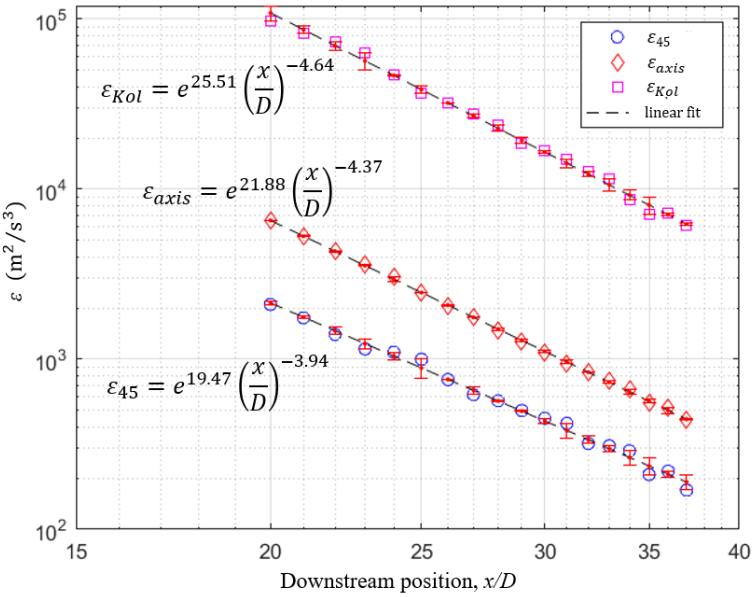

Fig. 14. Downstream evolution of the mean energy dissipation rate per unit mass, ε, in logarithmic scales with corresponding linear fits

5. Conclusions

In the current work, we have presented the centerline development of the main static and dynamic statistical quantities obtainable using a single component (streamwise oriented) laser Doppler anemometer throughout the developing and part of the developed region of a round turbulent jet. The employed laser Doppler anemometer has been built in-house and optimized for accurate measurements of fine-scale turbulence [14,34].

The statistics clearly show that the current jet becomes fully developed in both the first and second central statistical moments beyond approximately 25 jet exit diameters downstream of the jet exit. The second-order statistics take longer to develop fully than the first-order ones. The dynamic statistics show correspondingly that the spectra and second-order structure functions develop gradually until 30 jet exit diameters downstream of the jet exit has been reached. Beyond this limit, the jet displays (on average) a wide -5/3 range for the spectra and 2/3 region for the second-order structure functions. The measurements provide the time and length scales for the downstream development of the jet from the initial laminar uniform profile at the jet exit. These results can consequently be used for development and/or validation of turbulence models in a classical flow that at least on average displays the same physics as the Kolmogorov theory of turbulence, upon which the majority of current turbulence models are built.

It is also interesting that the linear fits of the mean velocity and the velocity variance appear to originate in different downstream positions, which will be further investigated in future publications.

Acknowledgement

The authors wish to acknowledge the support of Ministry of Education Malaysia, Universiti Teknikal Malaysia Melaka (UTeM), DTU Mechanical Engineering, Reinholdt W. Jorck og Hustrus Fond (grant journal no. 13-J9-0026), Fabriksejer, Civilingeniør Louis Dreyer Myhrwold og hustru Janne Myhrwolds Fond (grant journal no. 13-M7-0039, 15-M7-0031 and 17-M7-0035) and Siemens A/S Fond grant no. 41.

References

[1] Capp, Steven P. "EXPERIMENTAL INVESTIGATION OF THE TURBULENT AXISYMMETRIC JET." (1984): 2193-2193.
[2] Weisgraber, T. H., and D. Liepmann. "Turbulent structure during transition to self-similarity in a round jet." *Experiments in Fluids* 24, no. 3 (1998): 210-224.
[3] Wygnanski, Israel, and Ho Fiedler. "Some measurements in the self-preserving jet." *Journal of Fluid Mechanics* 38, no. 3 (1969): 577-612.
[4] Zarruk, G. A., and E. A. Cowen. "Simultaneous velocity and passive scalar concentration measurements in low Reynolds number neutrally buoyant turbulent round jets." *Experiments in Fluids* 44, no. 6 (2008): 865-872.
[5] Hussein, Hussein J., Steven P. Capp, and William K. George. "Velocity measurements in a high-Reynolds-number, momentum-conserving, axisymmetric, turbulent jet." *Journal of Fluid Mechanics* 258 (1994): 31-75.
[6] Panchapakesan, Nagangudy R., and John L. Lumley. "Turbulence measurements in axisymmetric jets of air and helium. Part 1. Air jet." *Journal of Fluid Mechanics* 246 (1993): 197-223.
[7] Richards, Cecilia D., and William M. Pitts. "Global density effects on the self-preservation behaviour of turbulent free jets." *Journal of Fluid Mechanics* 254 (1993): 417-435.
[8] Dowling, David R., and Paul E. Dimotakis. "Similarity of the concentration field of gas-phase turbulent jets." *Journal of Fluid Mechanics* 218 (1990): 109-141.
[9] George, William K., and Michael M. Gibson. "The self-preservation of homogeneous shear flow turbulence." *Experiments in fluids* 13, no. 4 (1992): 229-238.
[10] George, William K. "The decay of homogeneous isotropic turbulence." *Physics of Fluids A: Fluid Dynamics* 4, no. 7 (1992): 1492-1509.
[11] George, William K. "Asymptotic effect of initial and upstream conditions on turbulence." *Journal of Fluids Engineering* 134, no. 6 (2012): 061203.
[12] Velte, Clara Marika, William K. George, and Preben Buchhave. "Estimation of burst-mode LDA power spectra." *Experiments in fluids* 55, no. 3 (2014): 1674.
[13] Yaacob, Mohd Rusdy, Rasmus Korslund Schlander, Preben Buchhave, and Clara Marika Velte. "Mapping of the turbulent round jet developing region using a constant temperature anemometer (CTA)." *Malaysian Journal of Fundamental and Applied Sciences* Special Issue on Natural Sciences and Mathematics (ESCon 2018) (2018): 443-446.
[14] Yaacob, Mohd Rusdy, Rasmus Korslund Schlander, Preben Buchhave, and Clara Marika Velte. "Validation of improved laser Doppler anemometer (LDA) based on the fully developed turbulent round jet." In *Symposium on Electrical, Mechatronics and Applied Science 2018*. 2018.
[15] Buchhave, Preben, and Clara M. Velte. "Measurement of turbulent spatial structure and kinetic energy spectrum by exact temporal-to-spatial mapping." *Physics of Fluids* 29, no. 8 (2017): 085109.
[16] Mohd Rusdy Yaacob, Rasmus Korslund Schlander, Preben Buchhave and, Clara M.Velte. "Experimental Evaluation of Kolmogorov's -5/3 and 2/3 Power Laws in the Developing Turbulent Round Jet." *Journal of Advanced Research in Fluid Mechanics and Thermal Sciences* 45, no. 1 (2018): 14–21.
[17] Kolmogorov, Andrei Nikolaevitch. "On degeneration (decay) of isotropic turbulence in an incompressible viscous liquid." In *Dokl. Akad. Nauk SSSR*, vol. 31, pp. 538-540. 1941.
[18] Kolmogorov, Andrey Nikolaevich. "Dissipation of energy in locally isotropic turbulence." In *Akademiia Nauk SSSR Doklady*, vol. 32, p. 16. 1941.
[19] Kolmogorov, Andrei Nikolaevich. "The local structure of turbulence in incompressible viscous fluid for very large Reynolds numbers." *Proceedings of the Royal Society of London. Series A: Mathematical and Physical Sciences* 434, no. 1890 (1991): 9-13.
[20] Kolmogorov, Andrey Nikolaevich. "A refinement of previous hypotheses concerning the local structure of turbulence in a viscous incompressible fluid at high Reynolds number." *Journal of Fluid Mechanics* 13, no. 1 (1962): 82-85.
[21] Jung, Daehan. *An investigation of the Reynolds-number dependence of the axisymmetric jet mixing layer using a 138 hot-wire probe and the POD*. 2001.

[22] Bell, James H., and Rabindra D. Mehta. "Contraction design for small low-speed wind tunnels." (1988).
[23] Fellouah, H., C. G. Ball, and A. Pollard. "Reynolds number effects within the development region of a turbulent round free jet." *International Journal of Heat and Mass Transfer* 52, no. 17-18 (2009): 3943-3954.
[24] Melling, A. *Seeding gas flows for laser anemometry*. CRANFIELD INST OF TECH (ENGLAND) SCHOOL OF MECHANICAL ENGINEERING, 1986.
[25] Albrecht, H-E., Nils Damaschke, Michael Borys, and Cameron Tropea. *Laser Doppler and phase Doppler measurement techniques*. Springer Science & Business Media, 2013.
[26] Tropea, Cameron, and Alexander L. Yarin. *Springer handbook of experimental fluid mechanics*. Springer Science & Business Media, 2007.
[27] Bartleft, K. G., and C. Y. She. "Remote measurement of wind speed using a dual beam backscatter laser Doppler velocimeter." *Applied optics* 15, no. 8 (1976): 1980-1983.
[28] Grant, George R., and Kenneth L. Orloff. "Two-color dual-beam backscatter laser Doppler velocimeter." *Applied optics* 12, no. 12 (1973): 2913-2916.
[29] Sommerfeld, Martin, and Cameron Tropea. "Single-point laser measurement." In *Instrumentation for Fluid Particle Flow*, pp. 252-317. William Andrew Publishing, 1999.
[30] Diop, Moussa, Sébastien Piponniau, and Pierre Dupont. "High resolution LDA measurements in transitional oblique shock wave boundary layer interaction." *Experiments in Fluids* 60, no. 4 (2019): 57.
[31] Buchhave, P. "Three-component LDA measurements." *Disa Information* (1984): 3-9.
[32] Buchhave, Preben, and Clara M. Velte. "Reduction of noise and bias in randomly sampled power spectra." *Experiments in Fluids* 56, no. 4 (2015): 79.
[33] Fischer, Andreas. "Imaging flow velocimetry with laser Mie scattering." *Applied Sciences* 7, no. 12 (2017): 1298.
[34] Yaacob, Mohd Rusdy, Rasmus Korslund Schlander, Preben Buchhave, and Clara Marika Velte. "A novel laser Doppler anemometer (LDA) for high-accuracy turbulence measurements." *arXiv preprint arXiv:1905.08066* (2019).
[35] Buchhave, P. "Errors and correction methods in turbulence measurements with the LDA." *Proc. of LDV-III Laser Velocimetry in Hostile Environments* (1979): 221-229.
[36] Buchhave, Preben, William K. George Jr, and John L. Lumley. "The measurement of turbulence with the laser-Doppler anemometer." *Annual review of fluid mechanics* 11, no. 1 (1979): 443-503.
[37] Velte, Clara Marika, Martin Otto Laver Hansen, William K. George, and Knud Erik Meyer. *Characterization of vortex generator induced flow*. Technical University of Denmark, 2009.
[38] Lumley, J. L. "Interpretation of time spectra measured in high-intensity shear flows." *The physics of fluids* 8, no. 6 (1965): 1056-1062.
[39] Frisch, Uriel, and Andreĭ Nikolaevich Kolmogorov. *Turbulence: the legacy of AN Kolmogorov*. Cambridge university press, 1995.
[40] McDonough, James M. "Introductory lectures on turbulence: physics, mathematics and modeling." (2007).
[41] Wyngaard, J. C., and S. F. Clifford. "Taylor's hypothesis and high–frequency turbulence spectra." *Journal of the Atmospheric Sciences* 34, no. 6 (1977): 922-929.
[42] Grandchamp, Xavier, Annemie Van Hirtum, and Xavier Pelorson. "Centreline velocity decay characterisation in low-velocity jets downstream from an extended conical diffuser." *Meccanica* 48, no. 3 (2013): 567-583.
[43] Ball, C. G., H. Fellouah, and A. Pollard. "The flow field in turbulent round free jets." *Progress in Aerospace Sciences* 50 (2012): 1-26.
[44] Cant, R. S. "SB Pope, Turbulent Flows, Cambridge University Press, Cambridge, UK." *Combustion and Flame* 125 (2001): 1361-1362.
[45] Mi, J., D. S. Nobes, and G. J. Nathan. "Influence of jet exit conditions on the passive scalar field of an axisymmetric free jet." *Journal of Fluid Mechanics* 432 (2001): 91-125.
[46] A. Hodzic. *Experimental and theoretical investigations of turbulent axi-symmetric jets*. Technical University of Denmark, 2019.
[47] Kassab, Sadek Z., Ayman E. Bakry, and Hassan A. Warda. "Laser Doppler anemometry measurements in an axisymmetric turbulent jet." *Review of scientific instruments* 67, no. 5 (1996): 1842-1849.
[48] Ferdman, E., M. V. -Oslash, t-uacute, gen, and S. Kim. "Effect of initial velocity profile on the development of round jets." *Journal of Propulsion and Power* 16, no. 4 (2000): 676-686.
[49] Hodzic, A. "PIV measurements on a turbulent free jet-spatial decomposition of a turbulent free jet using proper orthogonal decomposition." PhD diss., Master thesis, Technical University of Denmark, Kgs. Lyngby, 2014.
[50] G. K. Batchelor. *The theory of homogeneous turbulence*. Cambridge University Press, 1953.
[51] Gibson, M. M. "Spectra of turbulence at high Reynolds number." *Nature* 195, no. 4848 (1962): 1281-1283.
[52] Buchhave, Preben, and Clara M. Velte. "Conversion of measured turbulence spectra from temporal to spatial domain." In *Whither Turbulence and Big Data in the 21st Century?*, pp. 343-362. Springer, Cham, 2017.
[53] Velte, Clara M., Preben Buchhave, and Azur Hodžić. "Measurement of Turbulent Spatial Structure and Kinetic

Energy Spectrum—Part 2: Convection Record Measurements." In *Progress in Turbulence VII*, pp. 171-176. Springer, Cham, 2017.
[54] Danaila, L., F. Anselmet, and R. A. Antonia. "An overview of the effect of large-scale inhomogeneities on small-scale turbulence." *Physics of Fluids* 14, no. 7 (2002): 2475-2484.
[55] Romano, Giovanni Paolo, and Robert A. Antonia. "Longitudinal and transverse structure functions in a turbulent round jet: effect of initial conditions and Reynolds number." *Journal of Fluid Mechanics* 436 (2001): 231-248.
[56] Fellouah, Hachimi, and Andrew Pollard. "The velocity spectra and turbulence length scale distributions in the near to intermediate regions of a round free turbulent jet." *Physics of Fluids* 21, no. 11 (2009): 115101.
[57] Tennekes, Hendrik, John Leask Lumley, and J. L. Lumley. *A first course in turbulence*. MIT press, 1972.
[58] George, William K., and Hussein J. Hussein. "Locally axisymmetric turbulence." *Journal of Fluid Mechanics* 233 (1991): 1-23.